Comparison of Turbulence Models for an Internal Flow with Side Wall Mass Injection

B. A. Sen, U. G. Yuksel and K. Kirkkopru
Faculty of Mechanical Engineering, Istanbul Technical University, Gumussuyu, Istanbul, Turkey

Introduction

Solid propellant rocket boosters (SPRB) are used extensively in aerospace activities when a strong thrust is needed as in the case of lifting off the satellites for space activities [1]. Flow structures occurring within the SPRB's have drawn the attention of the researchers either experimentally [2,3], or as it happens increasingly today, computationally [4,5]. The flow field inside the combustion chamber experiences different processes since the characteristic velocity throughout the chamber is on the order of Ma = $O(10^{-2})$ [6], whereas the exit velocity is supersonic. Time dependent behavior of various processes, turbulence, combustion, as well as with the compressibility effects add intricacy into the simulation processes. Today, major study field for the SPRBs is the flow stability problem inside the combustion chamber [6], and its interaction with combustion [7] and turbulence [8].

This study is the first part of an ongoing research held in the Faculty of Mechanical Engineering at Istanbul Technical University (ITU), to simulate the interaction of the turbulence, combustion and the acoustic field inside SPRBs. In this preliminary work, a computational study has been performed to identify the effect of various turbulence models on the calculations of cold flow field inside a model SPRB combustion chamber. A commercial flow solver, Fluent 6.1.22, has been employed for the computations.

The flow configuration chosen is an idealization of that found in a solid rocket motor, and was selected in accordance with the VECLA facility of ONERA that is an experimental set up for investigating the characteristics of injection driven flows [4,8,9]. Schematic of the facility is given in Figure 1, where the length of the channel is $L = 0.581$ m and its height is $h = 0.0103$ m. The channel is bounded at $y/h = 0$ by a permeable wall allowing the mass injection and at $y/h = 1$ by an impermeable wall. The upstream at $x/L = 0$, head-end, is closed and the downstream, at $x/L = 1$, exit section, is open to the atmosphere. Sidewall mass injection is used to mimic the normal velocity of gaseous products generated by combustion of gasified propellant.

For this particular work, based on the Reynolds averaged Navier Stokes equations, computations have been performed by modeling the turbulence with one equation model (Spallart Allmaras), two equation models (Standard k-ε, RNG k-ε, Realizable k-ε, SST k-ω) and the Reynolds Stress model. Set of governing equations has been solved by employing the Finite Volume technique [10]. Boundary conditions were specified as, air injection mass flux, $\dot{m} = 2.619$ kg/m^{2}s, and the appropriate turbulence quantities, $\tilde{k} = 0.0001$ m^2/s^2, $\tilde{\varepsilon} = 0.001$ m^2/s^3, $\tilde{\omega} = 0.4$ $1/s$, at the permeable wall; pressure outlet, 137400 Pa, in the exit section and no slip condition for the impermeable wall at $y/h = 1$ and the solid wall in the head-end, at $y/h = 0$. Reynolds number based on the injection velocity and the channel height, Re_i, is approximately 8000. Density was calculated by the ideal gas law, and hence air injection temperature, 300 K, was specified. Normalized longitudinal velocity and the turbulent intensity profiles calculated with various turbulence closure models are compared with those from the experiment reported in [9] at several cross sections.

Report Documentation Page

Form Approved
OMB No. 0704-0188

1. REPORT DATE	2. REPORT TYPE	3. DATES COVERED
22 JUN 2004	**N/A**	**-**

4. TITLE AND SUBTITLE	5a. CONTRACT NUMBER
Comparison of Turbulence Models for an Internal Flow with Side Wall Mass Injection	5b. GRANT NUMBER
	5c. PROGRAM ELEMENT NUMBER
6. AUTHOR(S)	5d. PROJECT NUMBER
	5e. TASK NUMBER
	5f. WORK UNIT NUMBER
7. PERFORMING ORGANIZATION NAME(S) AND ADDRESS(ES) **Istanbul Technical University, Gumussuyu, Istanbul, Turkey**	8. PERFORMING ORGANIZATION REPORT NUMBER
9. SPONSORING/MONITORING AGENCY NAME(S) AND ADDRESS(ES)	10. SPONSOR/MONITOR'S ACRONYM(S)
	11. SPONSOR/MONITOR'S REPORT NUMBER(S)

12. DISTRIBUTION/AVAILABILITY STATEMENT
Approved for public release, distribution unlimited

13. SUPPLEMENTARY NOTES
See also ADM001793, International Symposium on Energy Conversion Fundamentals Held in Istanbul, Turkey on 21-25 June 2005., The original document contains color images.

14. ABSTRACT

15. SUBJECT TERMS

16. SECURITY CLASSIFICATION OF:			17. LIMITATION OF ABSTRACT	18. NUMBER OF PAGES	19a. NAME OF RESPONSIBLE PERSON
a. REPORT	b. ABSTRACT	c. THIS PAGE			
unclassified	**unclassified**	**unclassified**	**UU**	**30**	

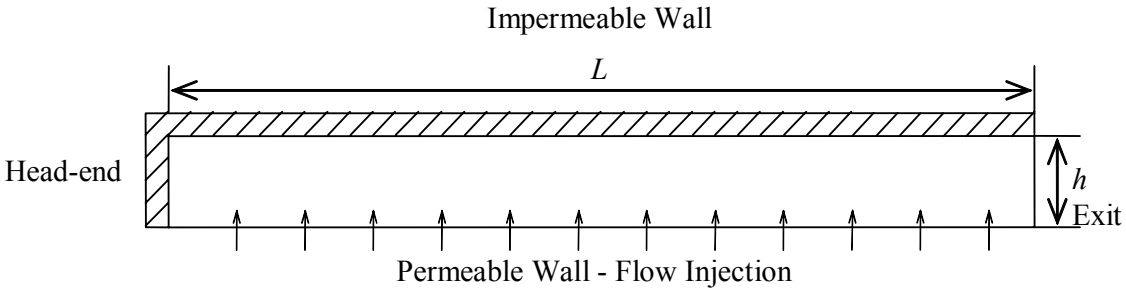

Figure 1. Schematic of computational domain

Results and Discussion

The injection Reynolds number was chosen as to produce a statistically stationary flow field and the first set of computations dealt with the comparison of the longitudinal velocity profiles obtained by steady and time marching feature of the FLUENT. It was shown that the profiles match excellently, allowing us to exploit the steady solver. In the next step, several turbulence closure models have been employed for computations and the calculated longitudinal velocity and turbulence intensity profiles were compared with those obtained from an experimental study reported by [9]. It is seen from Figure 2 that, Spalart-Allmaras turbulence closure model failed to compute satisfactory results. Computations based on the Reynolds stress model predicted the normalized longitudinal velocity profiles in a good agreement with the experiments. However, some discrepancy is detected in the neighborhood of the impermeable wall, hence; the validity of the closure model is questionable in this region. It was possible to acquire the longitudinal velocity profiles in the entire channel with a good accuracy with the SST k-ω model.

As given in Figure 3, the turbulence intensity levels obtained with the standard k-ε model failed to capture the experimental profiles. However, the turbulence intensity profiles obtained with the SST k-ω model are satisfactory, except for the second peak observed in the close neighborhood of the upper impermeable wall. Indeed, the accuracy of the experiment can be questionable in this region [9] because the existence of an impermeable wall may be expected to increase the turbulence levels in this region, leading to a possible peak.

The research grant from the Institute of Science and Technology of ITU and the CPU hours allocated by the Center of Excellence for Advanced Engineering Technologies are greatly acknowledged by the authors.

References

1. Sutton, G. P., *Rocket Propulsion Elements : An Introduction to the Engineering of Rockets*, John Wiley and Sons, New York, 1992
2. Traineau, J. C., Hervart, P. and Kuentzmann, P., "Cold-Flow Simulations of a Two-Dimensional Nozleless Solid Rocket Motor," AIAA Paper 86-1447, Jun. 1986
3. Dunlap, R., Blackner, A.M., Waugh, R.C., Brown, R.S. and Willoughby, P.G., "Internal Flow Field Studies in a Simulated Cylindrical Port Rocket Chamber". Journal of Propulsion and Power, Vol. 6, 1990, pp. 690-705.
4. Chaouat, B., "Numerical Simulation of Channel Flows with Fluid injection Using Reynolds Stress Model," AIAA Paper 2000-0992, Jan. 2000

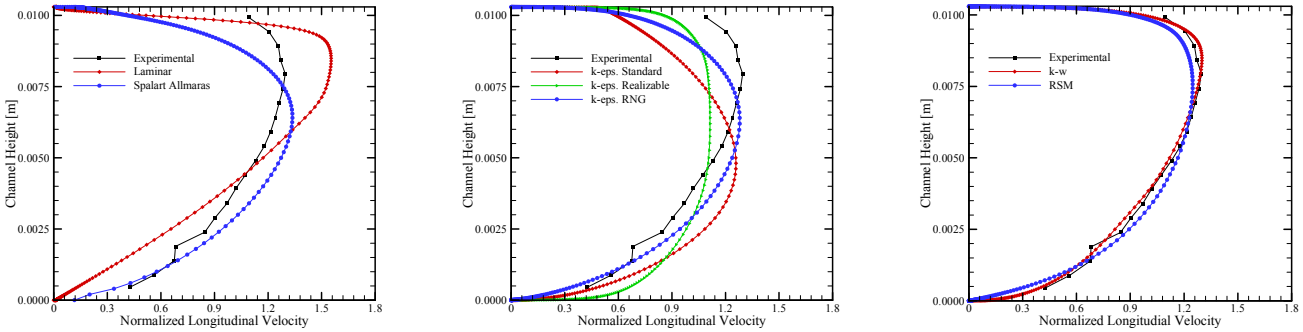

Figure 2. Normalized longitudinal velocity profiles, at $x = 0.500$ m, obtained with a) Laminar and Spalart-Allmaras, b) Standard k- ε, RNG k- ε and Realizable k- ε, c) Reynolds stress and SST k-ω closure models and from the experiment [9].

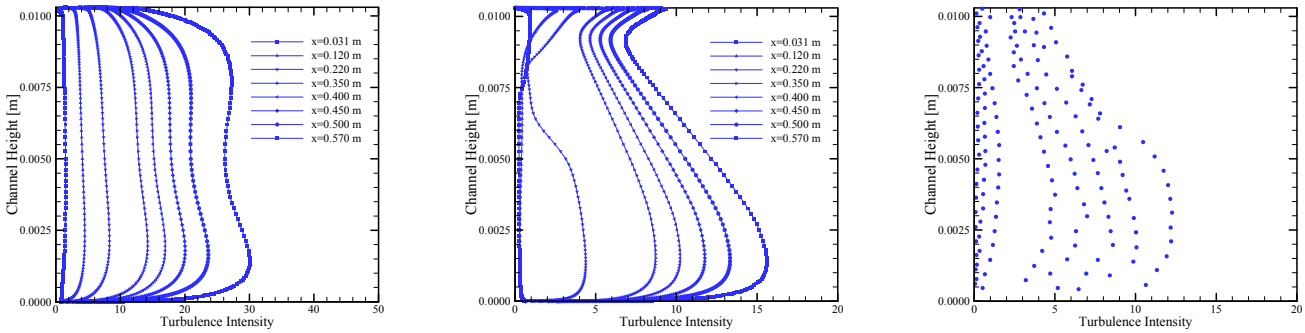

Figure 3. Turbulence intensity profiles obtained with a) Standard k- ε, b) SST k-ω and from c) Experiment [9].

5. Apte, S. and Yang, V., "Unsteady Flow Evolution and Combustion Dynamics of Homogeneous Solid Propellant in a Rocket Motor," Combustion and Flame, Vol. 131, 2002, pp. 110-131.
6. Kirkkopru, K., Kassoy, D.R., Zhao, Q. and Staab, P.L., "Acoustically Generated Unsteady Vorticity Field in a Long Narrow Cylinder with Sidewall Injection," Journal of Engineering Mathematics, Vol. 42, 2002, pp. 65-90.
7. Chu, W.-W., Yang, V. and Majdalani, J., "Premixed Flame Response to Acoustic Waves in a Porous-Walled Chamber with Surface Mass Injection," Combustion and Flame, Vol. 133, 2003, pp. 359-370.
8. Chaouat, B. and Schiestel, R., "Reynolds Stress Transport Modelling for Steady and Unsteady Channel Flows with Wall Injection," Journal of Turbulence, Vol. 3, 2002
9. Kourta, A., "Instability of Channel Flow with Surface Mass Injection and Paretial Vortex Shedding," Computers & Fluids, Vol. 33, 2004, pp. 155-178.
10. FLUENT 6.1 User's Guide, February 2003.

International Symposium on Energy Conversion Fundamentals
21-25 June 2004, Gumussuyu, Istanbul,TURKEY

Comparison of Turbulence Models for an Internal Flow with Side Wall Mass Injection

B. A. Sen U. G. Yuksel and K. Kirkkopru

Faculty of Mechanical Engineering,
Istanbul Technical University,
Gumussuyu, Istanbul, Turkey

Overview of the Presentation

- Introduction
- Governing Equations
- Numerical Models and Boundary Conditions
- Computational Results
- Conclusion

Major Mechanisms in SPRB Flow Evolution

- Local flow oscillations
- Combustion instability
- Acoustic disturbances

↓

Flow Instability

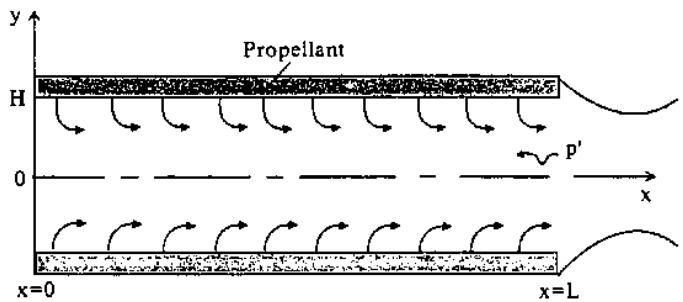

Figure 1. Schematic of a SPRB

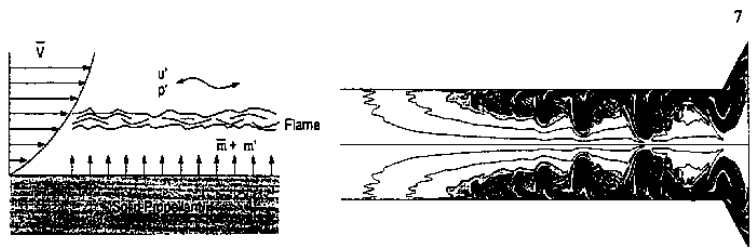

Figure 2. Unsteady flow evolution inside a SPRB
(V., Yang *et.al.* 1992-2004)
(Kirkkopru, K., Kassoy, D. R., 1996-2002)

Experimental Studies

- Traineau, J.-C., Hervart, P., Küntzmann, P., 1986.
- Dunlap, R., Blackner, A.M., Waugh, R.C., Brown, R.S., Willoughby, P.G., 1990.
- Vuillot, F., Scherrer, D., Habiballah, M., 2003.
- .....

Analytical and Computational Studies

- Culick, F. E.C., 1966.
- Vuillot, F., 1991.
- Vuillot, F., Avalon, G., 1991.
- Kirkkopru, K., Kassoy, D.R., Zhao, Q., Staab, P.L., 1996, 2002.
- .....

- Beddini, R.A., 1985.
- Chaouat, B., 2000.
- Chaouat, B., Schiestel, R. 2002.
- Kourta, A., 2004.
- Apte, S., Yang, V., 2000.
- Chu, W.-W., Yang, V., Majdalani, J., 2003.
- .....

Favre Averaged Equations

Reynolds Average

$$\overline{\Phi}(x,t) = \Phi(x,t) + \Phi'(x,t)$$

$$\Phi(x,t) = \lim_{T\to\infty} \frac{1}{T} \int_{t}^{t+T} \Phi(x,t)\,dt$$

Favre (Mass) Average

$$\Phi_i = \widetilde{\Phi}_i + \Phi_i''$$

$$\widetilde{\Phi} = \frac{1}{\overline{\rho}} \lim_{T\to\infty} \frac{1}{T} \int_{t}^{t+T} \rho(x,\tau)\Phi(x,\tau)\,d\tau$$

$$\widetilde{\Phi}(x,t) = \overline{\rho\overline{\Phi}(x,t)} \Big/ \overline{\rho}$$

Governing Equations

Continuity

$$\frac{\partial \overline{\rho}}{\partial t}+\frac{\partial}{\partial x_i}\left(\overline{\rho}\widetilde{u}_i\right)=0$$

Momentum

$$\frac{\partial}{\partial t}\left(\overline{\rho}\widetilde{u}_i\right)+\frac{\partial}{\partial x_j}\left(\overline{\rho}\widetilde{u}_j\widetilde{u}_i\right)=-\frac{\partial P}{\partial x_i}+\frac{\partial}{\partial x_j}\left[\overline{t}_{ji}-\overline{\rho u_j'' u_i''}\right]$$

Energy

$$\frac{\partial}{\partial t}\left[\overline{\rho}\left(\overline{e}+\frac{\widetilde{u}_i\widetilde{u}_i}{2}\right)+\frac{\overline{\rho u_i'' u_i''}}{2}\right]+\frac{\partial}{\partial x_j}\left[\overline{\rho}\widetilde{u}_j\left(\overline{h}+\frac{\widetilde{u}_i\widetilde{u}_i}{2}\right)+\widetilde{u}_j\frac{\overline{\rho u_i'' u_i''}}{2}\right]$$

$$=\frac{\partial}{\partial x_j}\left[-q_{Lj}-\overline{\rho u_i'' h''}+\overline{t_{ij}u_i''}-\overline{\rho u_j''\tfrac{1}{2}u_i'' u_i''}\right]+\frac{\partial}{\partial x_j}\left[\widetilde{u}_i\left(\overline{t}_{ij}-\overline{\rho u_j'' u_i''}\right)\right]$$

State Equation(Perfect Gas)

$$P=\overline{\rho}R\widetilde{T}$$

Turbulence Models

First Order Models

- Spalart Allmaras Model
- Standard *k-ε* model
- RNG *k-ε* model
- Realizable *k-ε* model
- SST k-omega model

Boussinesq approximation

$$-\overline{\rho u_j'' u_i''} = 2\mu_T \tilde{S}_{ji} - \left(\frac{2\mu_T}{3}\right)\frac{\partial \tilde{u}_k}{\partial x_k}\delta_{ji} - \frac{2}{3}\overline{\rho}\tilde{k}\delta_{ji}$$

Second Order Model

- Reynolds Stress Model

$$\overline{u_j'' u_i''}$$

Spalart Allmaras Model

Transport equation for $\tilde{\nu}$

$$\frac{\partial}{\partial t}(\bar{\rho}\tilde{\nu})+\frac{\partial}{\partial x_i}(\bar{\rho}\tilde{\nu}u_i)=C_{b1}\rho\left[S+\frac{\tilde{\nu}}{\kappa^2 d^2}\left(1-\frac{X}{1+Xf_{\nu 1}}\right)\right]+\frac{1}{\sigma_\nu}\left[\frac{\partial}{\partial x_j}\left((\mu+\rho\nu)\frac{\partial \nu}{\partial x_j}\right)+C_{b2}\rho\left(\frac{\partial \nu}{\partial x_j}\right)^2\right]-Y_\nu$$

Eddy viscosity $\mu_T=\rho\tilde{\nu}f_{\nu 1}$

$$f_{\nu 1}=\frac{X^3}{X^3+C^3{}_{\nu 1}}$$

Damping function

$$Y_\nu=C_{\omega 1}\rho g\left[\frac{1+C^6{}_{\omega 3}}{g^6+C^6{}_{\omega 3}}\right]^{1/6}$$

Destruction of the viscosity

$$X=\frac{\tilde{\nu}}{\nu}$$

Normalized eddy viscosity

Standard *k-ε* model

Turbulent kinetic energy

$$\frac{\partial}{\partial t}\left(\overline{\rho}\widetilde{k}\right)+\frac{\partial}{\partial x_i}\left(\overline{\rho}\widetilde{k}\widetilde{u}_i\right)=\frac{\partial}{\partial x_j}\left[\left(\mu+\frac{\mu_t}{\sigma_t}\right)\frac{\partial\widetilde{k}}{\partial x_j}\right]+\mu_T\widetilde{S}^2-\frac{1}{\overline{\rho}}g_i\frac{\mu_T}{\mathrm{Pr}_T}\left(\frac{\partial\overline{\rho}}{\partial\widetilde{T}}\right)_P\frac{\partial\widetilde{T}}{\partial x_i}+\overline{\rho}\widetilde{\varepsilon}-2\overline{\rho}\widetilde{\varepsilon}M_t^2$$

Dissipation of the turbulent kinetic energy

$$\frac{\partial}{\partial t}\left(\overline{\rho}\widetilde{\varepsilon}\right)+\frac{\partial}{\partial x_i}\left(\overline{\rho}\widetilde{\varepsilon}\widetilde{u}_i\right)=\frac{\partial}{\partial x_j}\left[\left(\mu+\frac{\mu_t}{\sigma_\varepsilon}\right)\frac{\partial\widetilde{\varepsilon}}{\partial x_j}\right]+C_{1\varepsilon}\frac{\widetilde{\varepsilon}}{\widetilde{k}}\left(\mu_T\widetilde{S}^2+C_{3\varepsilon}\left(-\frac{1}{\overline{\rho}}g_i\frac{\mu_T}{\mathrm{Pr}_T}\left(\frac{\partial\overline{\rho}}{\partial\widetilde{T}}\right)_P\frac{\partial\widetilde{T}}{\partial x_i}\right)\right)-C_{2\varepsilon}\overline{\rho}\frac{\widetilde{\varepsilon}^2}{\widetilde{k}}$$

Turbulent eddy viscosity

$$\mu_t=\overline{\rho}C_\mu\frac{\widetilde{k}^2}{\widetilde{\varepsilon}}$$

Turbulent Mach number

$$M_t^2=\sqrt{\frac{\widetilde{k}}{\gamma R\widetilde{T}}}$$

Modulus of the mean rate of strain tensor

$$\widetilde{S}=\sqrt{2\widetilde{S}_{ij}\widetilde{S}_{ij}}$$

Model coefficients

$C_{1\varepsilon}$	$C_{2\varepsilon}$	C_μ	σ_k	σ_ε
1.44	1.92	0.09	1.0	1.3

RNG *k-ε* model

Turbulent kinetic energy

$$\frac{\partial}{\partial t}\left(\bar{\rho}\tilde{k}\right)+\frac{\partial}{\partial x_i}\left(\bar{\rho}\tilde{k}\tilde{u}_i\right)=\frac{\partial}{\partial x_j}\left[\alpha_k\mu_{eff}\frac{\partial\tilde{k}}{\partial x_j}\right]+\mu_T\tilde{S}^2-\frac{1}{\bar{\rho}}g_i\frac{\mu_T}{\mathrm{Pr}_T}\left(\frac{\partial\bar{\rho}}{\partial\tilde{T}}\right)_P\frac{\partial\tilde{T}}{\partial x_i}+\bar{\rho}\tilde{\varepsilon}-2\bar{\rho}\tilde{\varepsilon}M_t^2$$

Dissipation of the turbulent kinetic energy

$$\frac{\partial}{\partial t}\left(\bar{\rho}\tilde{\varepsilon}\right)+\frac{\partial}{\partial x_i}\left(\bar{\rho}\tilde{\varepsilon}\tilde{u}_i\right)=\frac{\partial}{\partial x_j}\left[\alpha_\varepsilon\mu_{eff}\frac{\partial\tilde{\varepsilon}}{\partial x_j}\right]+C_{1\varepsilon}\frac{\tilde{\varepsilon}}{\tilde{k}}\left(\mu_T\tilde{S}^2+C_{3\varepsilon}\left(-\frac{1}{\bar{\rho}}g_i\frac{\mu_T}{\mathrm{Pr}_T}\left(\frac{\partial\tilde{\rho}}{\partial\tilde{T}}\right)_P\frac{\partial\tilde{T}}{\partial x_i}\right)\right)-C_{2\varepsilon}\bar{\rho}\frac{\tilde{\varepsilon}^2}{\tilde{k}}-R_\varepsilon$$

Additional destruction term

$$R_\varepsilon=\frac{C_\mu\bar{\rho}\tilde{\eta}^3\left(1-\eta/\eta_0\right)}{1+\beta\tilde{\eta}^3}\frac{\tilde{\varepsilon}^2}{\tilde{k}}$$

$$\tilde{\eta}\equiv\tilde{S}\tilde{k}\,/\,\tilde{\varepsilon}$$

$$\eta_0=4.38$$

$$\beta=0.012$$

Model coefficients

$C_{1\varepsilon}$	$C_{2\varepsilon}$	C_μ	σ_k	σ_ε
1.44	1.92	0.09	0.72	0.72

Realizable *k-ε* model

Turbulent kinetic energy

$$\frac{\partial}{\partial t}\left(\overline{\rho}\widetilde{k}\right)+\frac{\partial}{\partial x_i}\left(\overline{\rho}\widetilde{k}\widetilde{u}_j\right)=\frac{\partial}{\partial x_j}\left[\left(\mu+\frac{\mu_t}{\sigma_k}\right)\frac{\partial\widetilde{k}}{\partial x_j}\right]+\mu_T\widetilde{S}^2-\frac{1}{\overline{\rho}}g_i\frac{\mu_T}{\mathrm{Pr}_T}\left(\frac{\partial\overline{\rho}}{\partial\widetilde{T}}\right)_P\frac{\partial\widetilde{T}}{\partial x_i}-\overline{\rho}\widetilde{\varepsilon}-2\overline{\rho}\widetilde{\varepsilon}M_t^2$$

Dissipation of the turbulent kinetic energy

$$\frac{\partial}{\partial t}\left(\overline{\rho}\widetilde{\varepsilon}\right)+\frac{\partial}{\partial x_i}\left(\overline{\rho}\widetilde{\varepsilon}\widetilde{u}_j\right)=\frac{\partial}{\partial x_j}\left[\left(\mu+\frac{\mu_t}{\sigma_\varepsilon}\right)\frac{\partial\widetilde{\varepsilon}}{\partial x_j}\right]+C_1\overline{\rho}\widetilde{S}\widetilde{\varepsilon}-C_2\overline{\rho}\frac{\widetilde{\varepsilon}^2}{\widetilde{k}+\sqrt{\upsilon\widetilde{\varepsilon}}}+C_{1\varepsilon}\frac{\widetilde{\varepsilon}}{\widetilde{k}}C_{3\varepsilon}\left(-\frac{1}{\overline{\rho}}g_i\frac{\mu_T}{\mathrm{Pr}_T}\left(\frac{\partial\overline{\rho}}{\partial\widetilde{T}}\right)_P\frac{\partial\widetilde{T}}{\partial x_i}\right)$$

$$C_\mu=\frac{1}{A_0+A_S\dfrac{\widetilde{u}^*\widetilde{k}}{\widetilde{\varepsilon}}}\qquad C_1=\max\left[0.43,\frac{\widetilde{\eta}}{\widetilde{\eta}+5}\right]\qquad\widetilde{\eta}=\widetilde{S}\frac{\widetilde{k}}{\widetilde{\varepsilon}}$$

Model coefficients

$C_{1\varepsilon}$	C_2	σ_k	σ_ε
1.44	1.9	1.0	1.2

SST k-omega model

Turbulent kinetic energy

$$\frac{\partial}{\partial t}\left(\bar{\rho}\tilde{k}\right)+\frac{\partial}{\partial x_i}\left(\bar{\rho}\tilde{k}\tilde{u}_i\right)=\frac{\partial}{\partial x_j}\left[\Gamma_k\frac{\partial\tilde{k}}{\partial x_j}\right]+\mu_T\tilde{S}^2-\bar{\rho}\beta^* f_{B*}\tilde{k}\tilde{\omega}$$

Specific dissipation rate

$$\frac{\partial}{\partial t}\left(\bar{\rho}\tilde{\omega}\right)+\frac{\partial}{\partial x_i}\left(\bar{\rho}\tilde{\omega}\tilde{u}_i\right)=\frac{\partial}{\partial x_j}\left[\Gamma_\omega\frac{\partial\tilde{\omega}}{\partial x_j}\right]+\alpha\frac{\tilde{\omega}}{\tilde{k}}\mu_t\tilde{S}^2-\bar{\rho}\beta f_B\tilde{\omega}^2+2(1-F_1)\bar{\rho}\sigma_{\omega,2}\frac{1}{\tilde{\omega}}\frac{\partial\tilde{k}}{\partial x_j}\frac{\partial\tilde{\omega}}{\partial x_j}$$

Turbulent eddy viscosity $\mu_t=\alpha^*\dfrac{\rho k}{\omega}$

Effective diffusivities

$$\Gamma_k=\mu+\frac{\mu_t}{\sigma_k}$$

$$\Gamma_\omega=\mu+\frac{\mu_t}{\sigma_\omega}$$

Turbulent Prandtl numbers

$$\sigma_k=\frac{1}{F_1/\sigma_{k,1}+(1-F_1)/\sigma_{k,2}}$$

$$\sigma_\omega=\frac{1}{F_1/\sigma_{\omega,1}+(1-F_1)/\sigma_{\omega,2}}$$

SST k-omega model

Functions and Coefficients of dissipation of k

$$f_\beta^* = \begin{cases} 1 & \chi_k \le 0 \\ \dfrac{1+680\chi_k^2}{1+400\chi_k^2} & \chi_k > 0 \end{cases} \qquad \chi_k = \frac{1}{\omega^3}\frac{\partial k}{\partial x_j}\frac{\partial \omega}{\partial x_j}$$

$$\beta^* = \beta_i^*\left[1+\zeta^* F(M_t)\right] \qquad \beta_i^* = \beta_\infty^*\left(\frac{4/15+(\mathrm{Re}_t/R_B)^4}{1+(\mathrm{Re}_t/R_B)^4}\right)$$

$$\zeta^* = 1.5 \qquad R_B = 8 \qquad \beta_\infty^* = 0.09$$

Functions and Coefficients of dissipation of ω

$$f_\beta = \frac{1+70\chi_\omega}{1+80\chi_\omega} \qquad \chi_\omega = \left|\frac{\Omega_{ij}\Omega_{ji}S_{ki}}{(\beta_\infty^*\omega)^3}\right| \qquad \beta = \beta_i\left[1-\frac{\beta_i^*}{\beta_i}\zeta^* F(M_t)\right]$$

Functions for calculation of turbulent viscosity

$$\alpha^* = \alpha_\infty\left(\frac{\alpha_0^*+\mathrm{Re}_t/R_k}{1+\mathrm{Re}_t/R_k}\right) \qquad \alpha = \frac{\alpha_\infty}{\alpha^*}\left(\frac{\alpha_0+\mathrm{Re}_t/R_\omega}{1+\mathrm{Re}_t/R_\omega}\right) \qquad \mathrm{Re}_t = \frac{\rho k}{\mu\omega}$$

$$R_k = 6 \qquad \alpha_0^* = \beta_i/3$$

Reynolds Stress Model

Reynolds Stress Equation

$$\frac{\partial}{\partial t}\left(\overline{\rho}\widetilde{\tau}_{ij}^{R}\right)+\frac{\partial}{\partial x_k}\left(\overline{\rho}\widetilde{u}_k\widetilde{\tau}_{ij}^{R}\right)=-\frac{\partial}{\partial x_k}\left(\frac{\mu_t}{\sigma_t}\frac{\partial\widetilde{\tau}_{ij}^{R}}{\partial x_k}\right)+\frac{\partial}{\partial x_k}\left[\mu\frac{\partial\widetilde{\tau}_{ij}^{R}}{\partial x_k}\right]-\overline{\rho}\left(\widetilde{\tau}_{ik}^{R}\frac{\partial\widetilde{u}_j}{\partial x_k}+\widetilde{\tau}_{jk}^{R}\frac{\partial\widetilde{u}_i}{\partial x_k}\right)$$

$$-\frac{\mu_t}{\overline{\rho}\,\mathrm{Pr}_t}\left(g_i\frac{\partial\overline{\rho}}{\partial x_j}+g_J\frac{\partial\overline{\rho}}{\partial x_I}\right)+\phi_{ij}-\varepsilon_{ij}-2\overline{\rho}\Omega_k\left(\widetilde{\tau}^{R}{}_{jm}\widetilde{\varepsilon}_{ikm}+\widetilde{\tau}^{R}{}_{jm}\widetilde{\varepsilon}_{jkm}\right)$$

Turbulence viscosity

$$\mu_t=\overline{\rho}C_\mu\frac{\widetilde{k}^2}{\widetilde{\varepsilon}}$$

Dissipation tensor

$$\varepsilon_{ij}=\frac{2}{3}\delta_{ij}\left(\overline{\rho}\varepsilon+Y_M\right)$$

Pressure strain term

$$\widetilde{\Phi}_{ij}=\widetilde{\Phi}_{ij,1}+\widetilde{\Phi}_{ij,2}+\widetilde{\Phi}_{ij,w}$$

$$\widetilde{\Phi}_{ij,1}=-C_1\overline{\rho}\frac{\widetilde{\varepsilon}}{\widetilde{k}}\left[\widetilde{\tau}_{ij}^{R}-\frac{2}{3}\delta_{ij}\widetilde{k}\right]$$

$$\widetilde{\Phi}_{ij,2}=-C_2\left[\left(\widetilde{P}_{ij}+\widetilde{F}_{ij}+\widetilde{G}_{ij}-\widetilde{C}_{ij}\right)-\frac{1}{3}\delta_{ij}\left(\widetilde{P}_{kk}+\widetilde{G}_{kk}-\widetilde{C}_{kk}\right)\right]$$

$$\widetilde{\Phi}_{ij,\omega}=-C^{0}{}_{1}\frac{\widetilde{\varepsilon}}{\widetilde{k}}\left(\widetilde{\tau}_{km}^{R}n_kn_m\delta_{ij}-\frac{3}{2}\widetilde{\tau}_{ik}^{R}n_jn_k-\frac{3}{2}\widetilde{\tau}_{jk}^{R}n_in_k\right)\frac{\widetilde{k}^{3/2}}{C_{\rho\varepsilon d}}+C_2'\frac{\varepsilon}{k}\left(\widetilde{\phi}_{km,2}n_kn_m\delta_{ij}-\frac{3}{2}\widetilde{\phi}_{ik,2}n_jn_k-\frac{3}{2}\widetilde{\phi}_{jk,2}n_in_k\right)\frac{\widetilde{k}^{3/2}}{C_{\rho\varepsilon d}}$$

Computational Domain

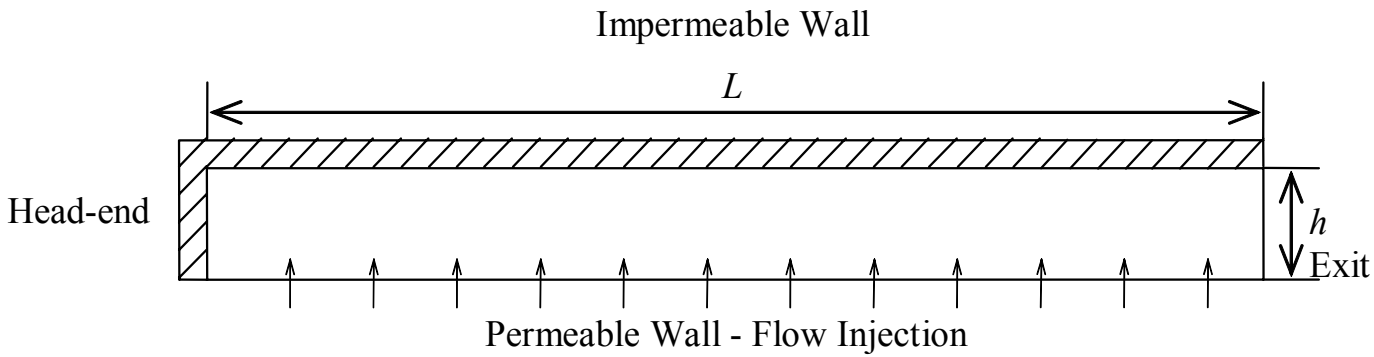

Schematics of the Vecla Facilty

L = 0.581 m h = 0.0103 m

Common Boundary Conditions

Injection Surface:

$\dot{m} = 2.619\, kg/m^2 s$

$T = 300 K$

Exit Surface:

$P = 137400 Pa$

- Chaouat, B., 2000.
- Kourta, A., 2004.

Turbulence Model Specific Inlet Conditions

k-ε models

$k = 0.0001\, m^2/s^2$

$\varepsilon = 0.001\, m^2/s^3$

k-ω model

$k = 0.0001\, m^2/s^2$

$\omega = 0.4 s^{-1}$

RSM

$\overline{v''v''} = 0.092\, m^2/s^2$

Computational Domain

Finite Volume Method (FLUENT)
Simple for Pressure velocity coupling
Second order upwind for remaining equations

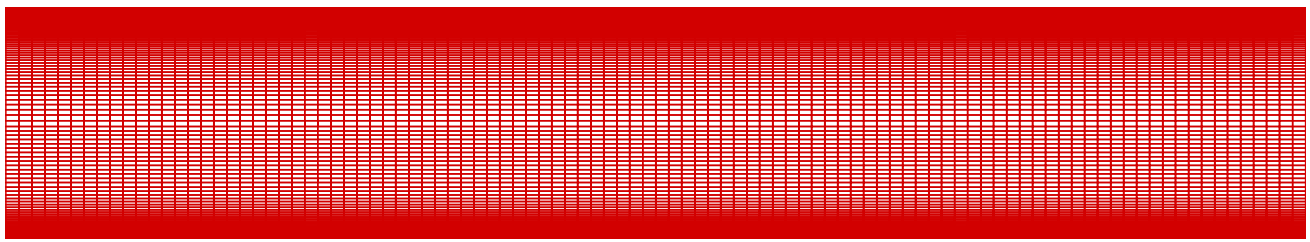

100 x 290 mesh points in *x* and *y* for steady calculations
100 x 242 mesh points in *x* and *y* for unsteady calculations

Time Marching Approach

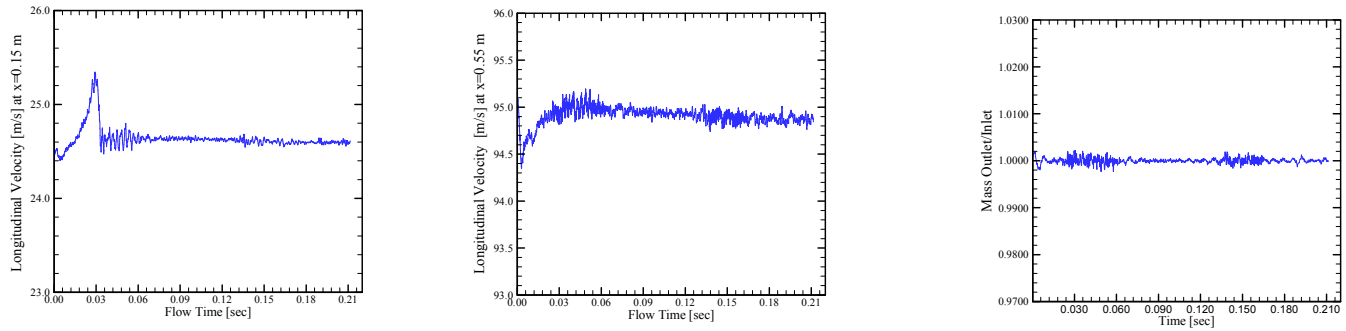

Time history for longitudinal velocity at sections a) 0.150 m, b) 0.55 m at mid height, and c) outlet to inlet mass flux ratio, obtained by time marching approach.

SST k-ω model has been used for time marching computations

Time Marching–Steady Approaches

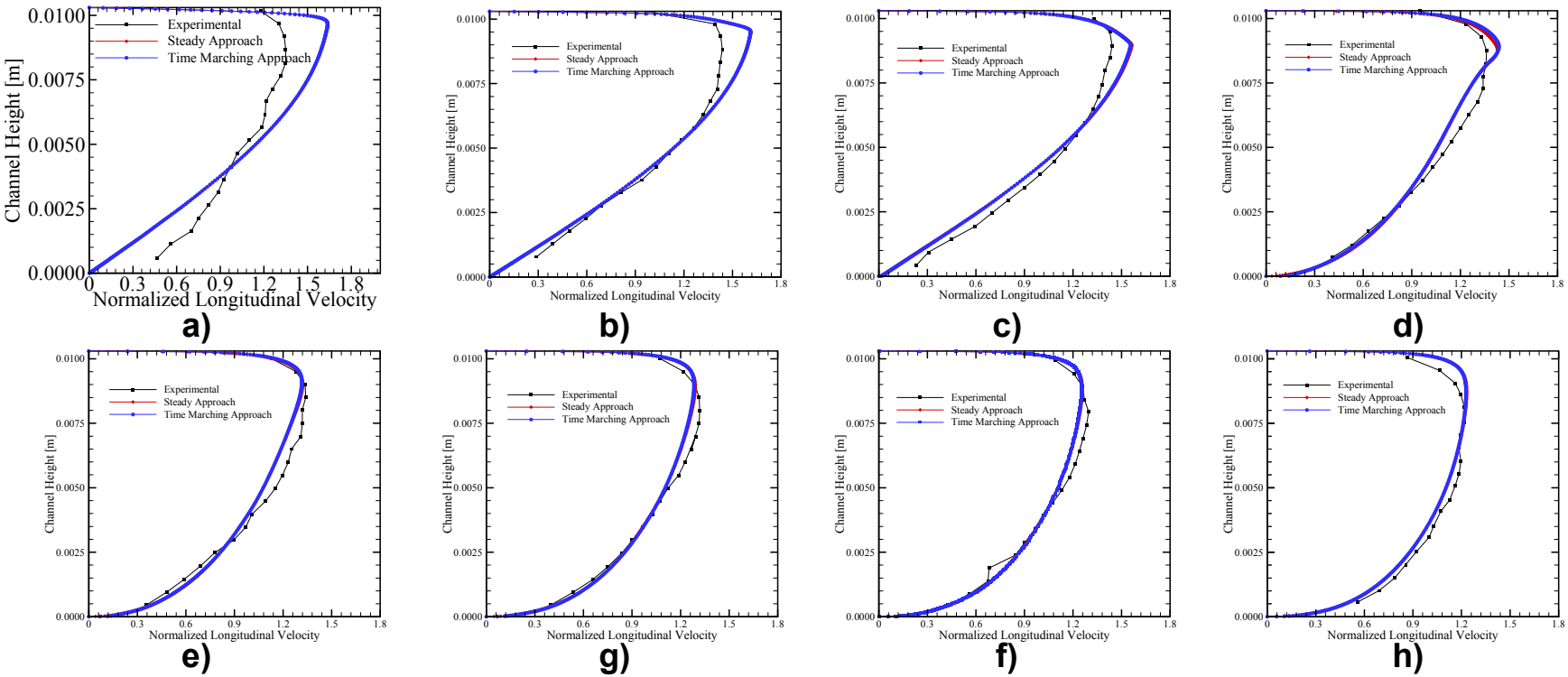

Comparison of the normalized longitudinal velocity distributions obtained by time marching and steady schemes at sections a) 0.031 m, b) 0.120 m., c) 0.220 m., d) 0.350 m., e)0.400 m., f) 0.450 m., g) 0.500 m. and h) 0.570 m. for the coarse mesh.

SST k-ω model has been used for comparison

Laminar and Spalart Allmaras

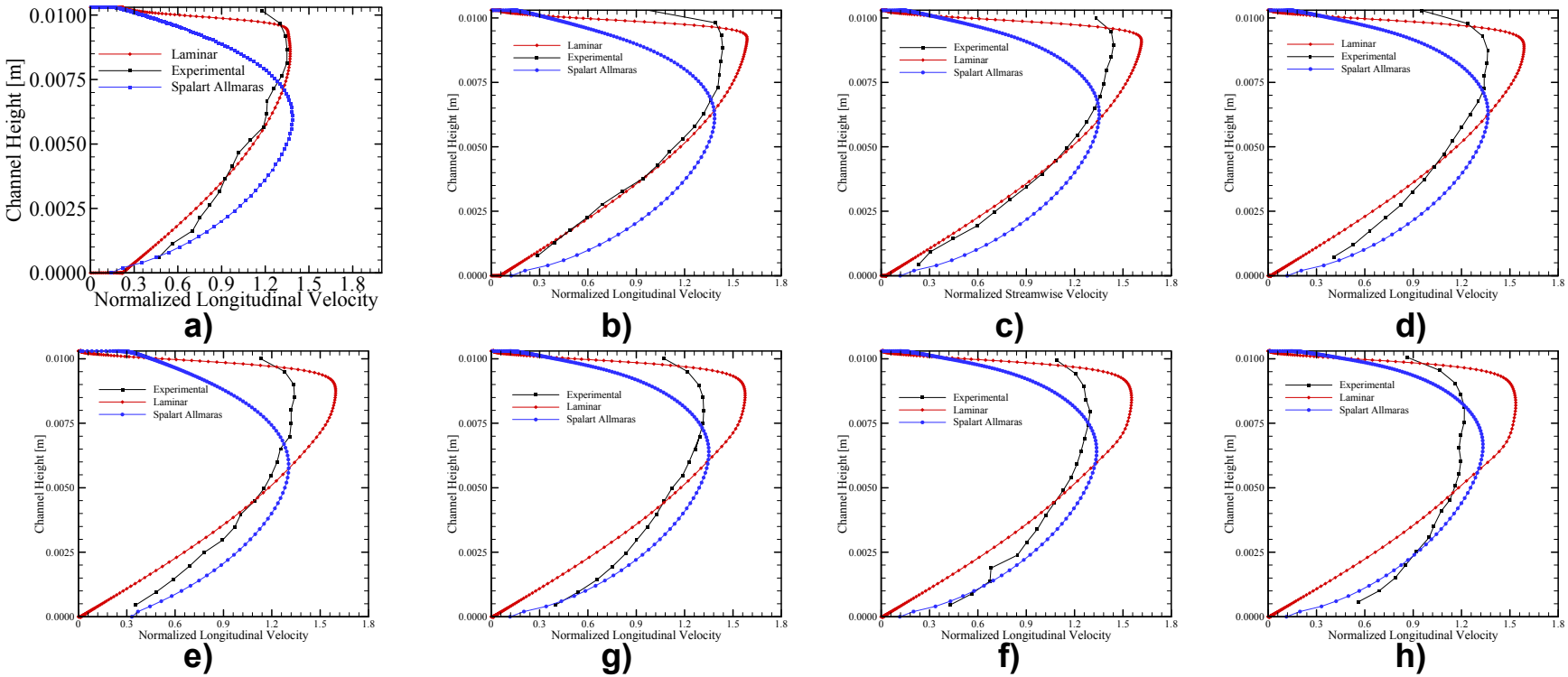

Normalized longitudinal velocity profiles obtained with the Laminar approach , the Spalart Allmaras turbulence closure model and from the experiment [3] at sections a) 0.031 m, b) 0.120 m., c) 0.220 m., d) 0.350 m., e)0.400 m., f) 0.450 m., g) 0.500 m. and h) 0.570 m. for the fine mesh.

Computations with *k-ε* based

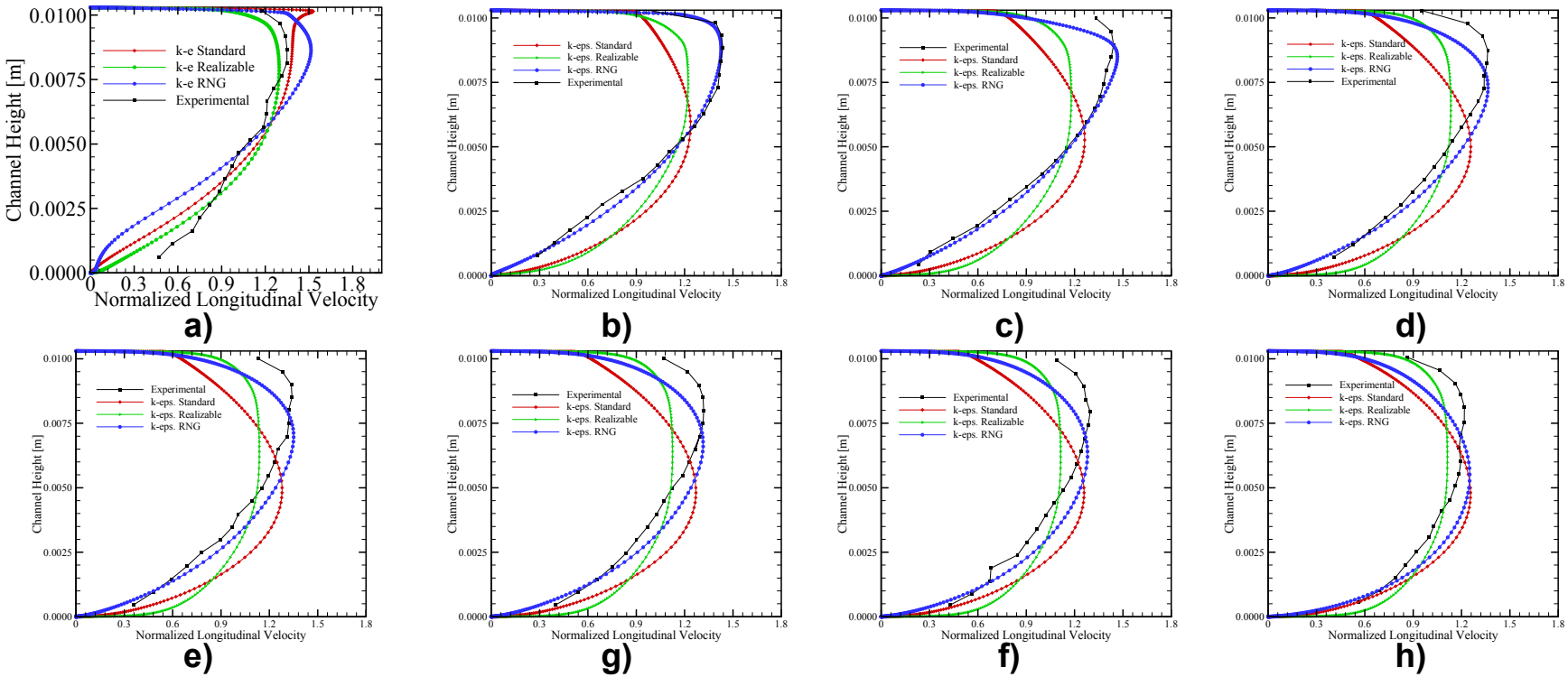

Normalized longitudinal velocity profiles obtained by the Standard *k- ε*, RNG *k-ε*, Realizable *k-ε* turbulence closure models and from experiment at sections a) 0.031 m, b) 0.120 m., c) 0.220 m., d) 0.350 m., e)0.400 m., f) 0.450 m., g) 0.500 m. and h) 0.570 m. for the fine mesh.

Reynolds Stress Model

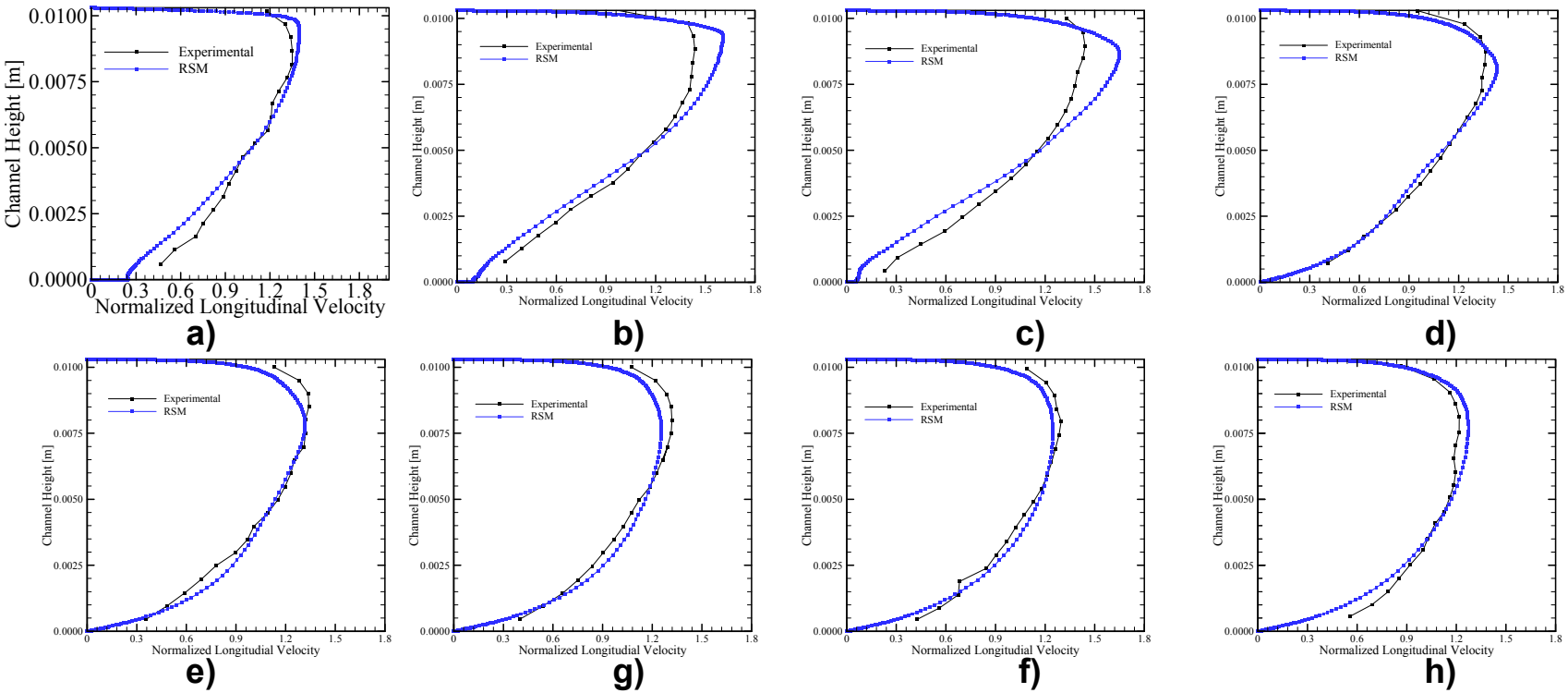

Normalized longitudinal velocity profiles obtained with the Reynolds Stress turbulence closure model and from experiment at sections a) 0.031 m, b) 0.120 m., c) 0.220 m., d) 0.350 m., e)0.400 m., f) 0.450 m., g) 0.500 m. and h) 0.570 m. for the fine mesh.

SST k-omega

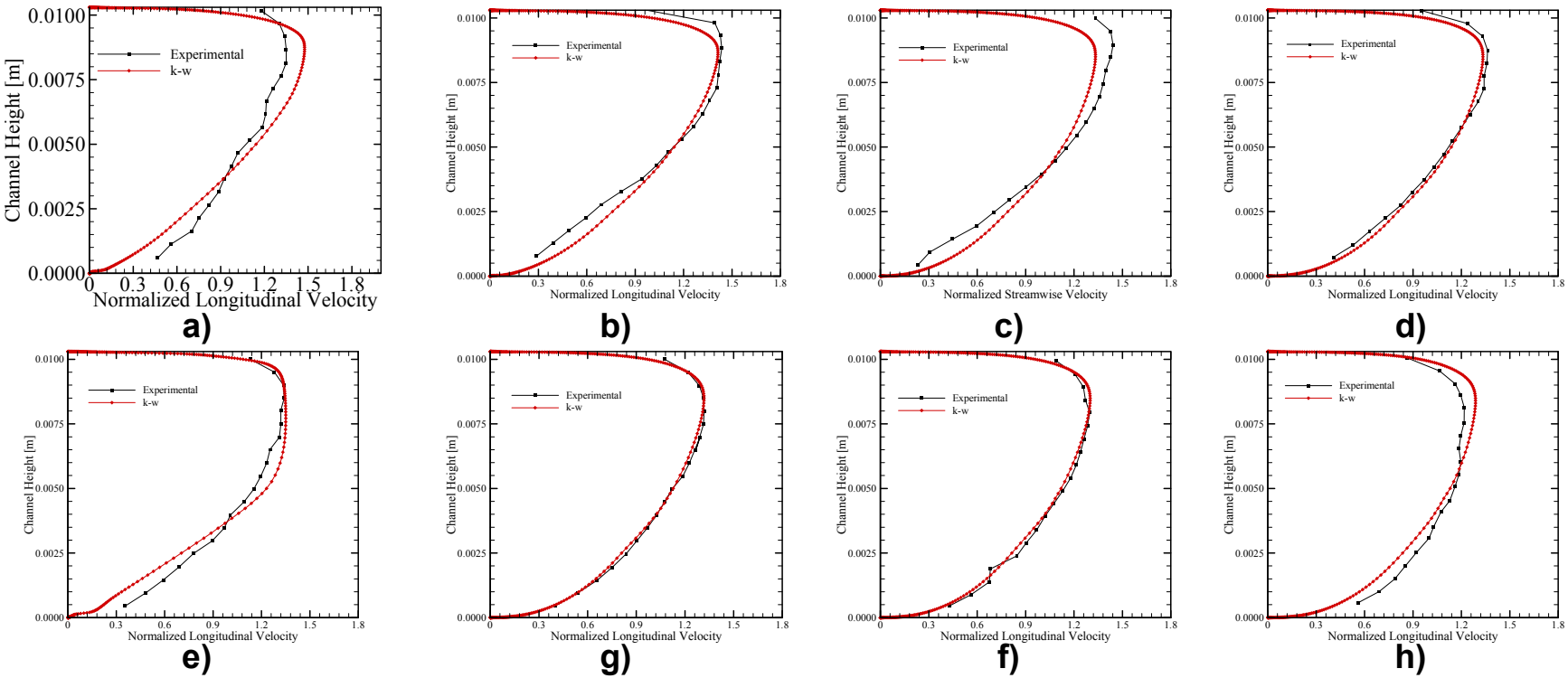

Normalized longitudinal velocity profiles obtained by the SST *k-ω* turbulence closure model and from experiment at sections a) 0.031 m, b) 0.120 m., c) 0.220 m., d) 0.350 m., e)0.400 m., f) 0.450 m., g) 0.500 m. and h) 0.570 m. for the fine mesh.

Turbulence Intensity

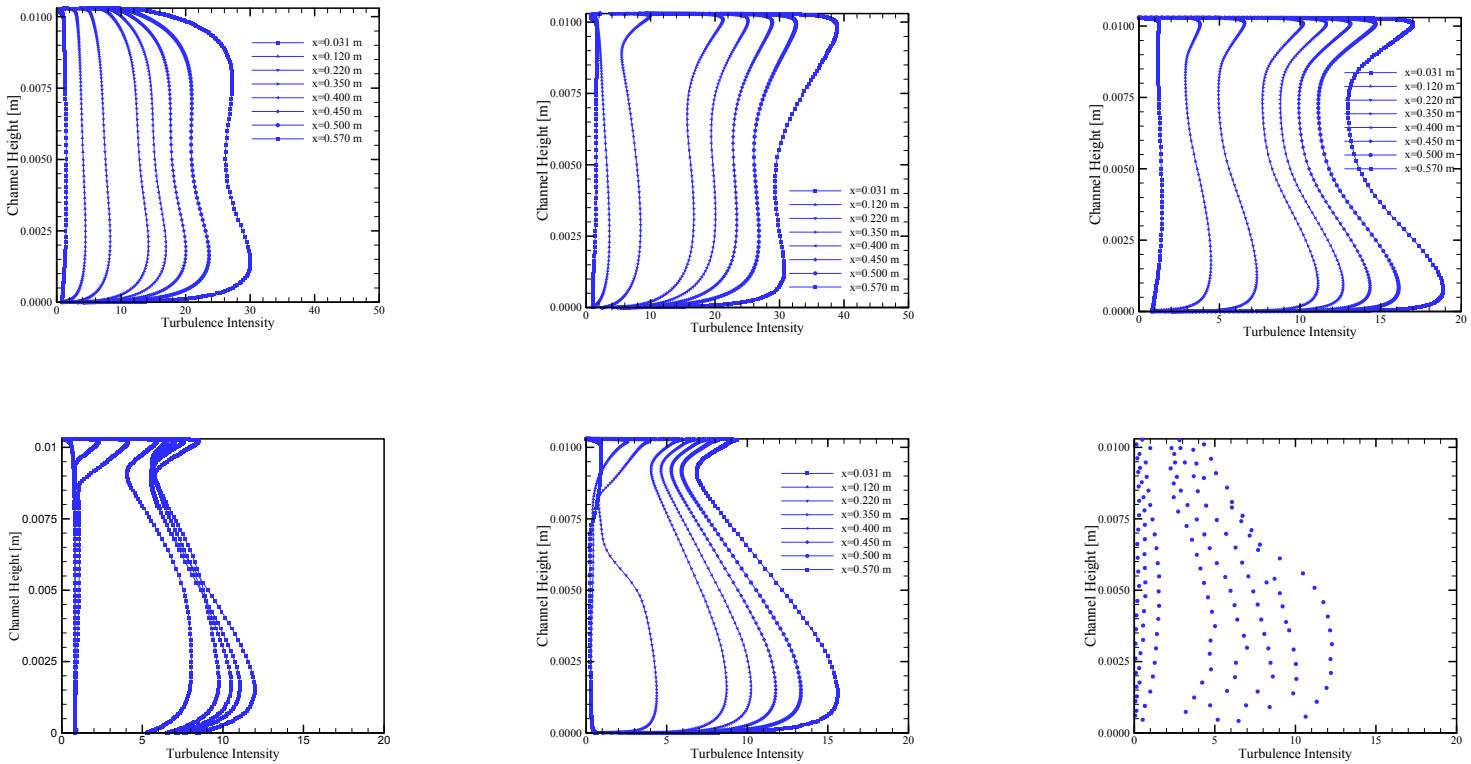

Turbulence intensity profiles obtained with the a) Standard *k-ε*, b) RNG *k-ε*, c) Realizable *k-ε*, d) Reynolds stress, e) SST *k-ω* turbulence closure models and f) from experiment, at eight sections

Results

• *k-ε* based computations have not produced velocity and turbulence intensity profiles compatible with the experimental profiles, neither in the pre (laminar) nor post-transition (turbulent) sections.

• Computations based on the Reynolds Stress Model have predicted the normalized longitudinal velocity profiles well except for the laminar region, and turbulence intensity profiles are similar qualitatively as those from the experiments.

• SST *k-ω* turbulence closure model has yielded the longitudinal velocity profiles in a good agreement with the experiment [3]. Furthermore, accuracy of the turbulence intensity profiles was satisfactory compared with the results from the rest of the closure models.

The research grant from the Institute of Science and Technology of ITU and the CPU hours allocated by the Center of Excellence for Advanced Engineering Technologies at ITU are greatly acknowledged by the authors.

References

1. Sutton, G. P., *Rocket Propulsion Elements : An Introduction to the Engineering of Rockets*, John Wiley and Sons, New York, 1992
2. Traineau, J. C., Hervart, P. and Kuentzmann, P., "Cold-Flow Simulations of a Two-Dimensional Nozeless Solid Rocket Motor," AIAA Paper 86-1447. 1986.
3. Dunlap, R., Blackner, A.M., Waugh, R.C., Brown, R.S. and Willoughby, P.G., "Internal Flow Field Studies in a Simulated Cylindrical Port Rocket Chamber," Journal of Propulsion and Power, Vol. 6, 1990, pp. 690-705.
4. Vuillot, F., Scherrer, D. and Habiballah, M., "CFD Code Validation for Space Propulsion Applications," 5th International Symposium on Liquid Space Propulsion-Longlife Combusition Devices Technology, Chattanooga, USA 27-30 October 2003.
5. Kourta, A., "Instability of Channel Flow with Surface Mass Injection and Parietal Vortex Shedding," Computers & Fluids, Vol. 33, 2004, pp. 155-178.
6. Chaouat, B. and Schiestel, R. "Reynolds Stress Transport Modeling for Steady and Unsteady Channel Flows with Wall Injection," Journal of Turbulence, Vol3, 2002
7. Sabnis, J.S., Madabhushi, R.K., Gibeling, H.J. and MacDonald, H., "On the Use of k- ε Turbulence model for Computation of Solid Rocket Internal Flows, AIAA Paper 89-2558, 1989.
8. Beddini, R.A., "Injection Induced Flows in Porous-Walled Ducts. AIAA Journal, Vol. 24, 1985, pp. 1766-1773.

References

9. Culick, F. E.C., “Rotational Axisymmetric Mean Flow and Damping of Acoustic Waves in Solid Propellant Rocket Motors,” AIAA Journal, Vol. 4, 1966, pp. 1462-1464.
10. Chaouat, B., “Numerical Simulation of Channel Flows with Fluid injection Using Reynolds Stress Model,” AIAA Paper 2000-0992, 2000.
11. Vuillot, F.,” Numerical Computation of Acoustic Boundary Layers in Large Solid Propellant Space Boosters,” AIAA Paper 91-0206, 1991
12. Vuillot, F., Avalon, G., “Acoustic Boundary Layers in Solid Propellant Rocket Motors Using Navier-Stokes Equations,” Journal of Propulsion and Power, Vol. 7, 1991, pp. 231-239.
13. Kirkkopru, K., Kassoy, D.R., Zhao, Q. and Staab, P.L., “Acoustically Generated Unsteady Vorticity Field in a Long Narrow Cylinder with Sidewall Injection,” Journal of Engineering Mathematics, Vol. 42, 2002, pp. 65-90.
14. Apte, S. and Yang, V., “Unsteady Flow Evolution and Combustion Dynamics of Homogeneous Solid Propellant in a Rocket Motor,” Combustion and Flame, Vol. 131, 2002, pp. 110-131.
15. Chu, W.-W., Yang, V., Majdalani, J., “Premixed Flame Response to Acoustic Waves in a Porous-Walled Chamber with Surface Mass Injection,” Combustion and Flame, Vol. 133, 2003, pp. 359-370.
16. FLUENT 6.1 User’s Guide, February 2003